

Quantum Error Correction Without Encoding via the Circulant Structure of Pauli Noise and the Fast Fourier Transform

Alvin Gonzales^{1*}

¹*Mathematics and Computer Science Division, Argonne National Laboratory, Lemont, IL, USA*

(Dated: January 9, 2025)

This work introduces a method for correcting the output distribution of a quantum computer that does not require encoding of the logical qubits into more physical qubits. Thus, it avoids the encoding overhead of standard quantum error correction codes. If the noise affecting the circuit is a Pauli channel (we can bias the noise with twirling), the ideal output distribution and noisy distribution in the standard basis are related by a stochastic matrix. We prove that this matrix has a circulant block structure. Thus, the ideal distribution can be retrieved from the noisy output distribution by applying the Fast Fourier Transform. Moreover, due to its circulant structure, characterization of this matrix can be achieved by sampling a single circuit. The results are corroborated with quantum hardware executions consisting of 20-qubit and 30-qubit GHZ state preparation, 5-qubit Grover, 6-qubit and 10-qubit quantum phase estimation, and 10-qubit and 20-qubit Dicke state preparation circuits. The correction process dramatically improves the accuracies of the output distributions. For 30-qubit GHZ state preparation, a corrected distribution fidelity of 97.7% is achieved from an initial raw fidelity of 23.2%.

I. INTRODUCTION

Quantum error correction codes (QECC) [1–3] are the standard approach for achieving reliable quantum computing. In fault tolerant quantum error correction, we can suppress the error rates to arbitrarily low levels provided that the physical error rates are below the code threshold [4]. The threshold requirement imposes a large overhead on the resources required for quantum computing. While progress has been made [5], fault tolerant quantum devices with many logical qubits are still far from reality with some estimates projecting that thousands of physical qubits are required for each logical qubit [6–8]. In its place, a suite of quantum error mitigation techniques are commonly used, where the goal is to improve results by reducing the effect of errors [9–16].

In QECC the goal is to correct the quantum state. However, in most quantum computing scenarios, the end goal is to generate accurate results which can be described by an output distribution or expectation value. Thus, in many cases, correcting the quantum state is overkill. For instance, the Bell states $|\Phi^\pm\rangle = \frac{1}{\sqrt{2}}(|00\rangle \pm |11\rangle)$ generate the same distribution in the standard basis and the relative phase is irrelevant. If we instead focus on correcting the output distribution, it is intuitive that we can achieve substantial savings in resources. This work verifies that this intuition is correct. A novel quantum error correction (QEC) approach is introduced that does not involve encoding of logical states into more physical qubits, but instead leverages the circulant structure of Pauli noise and the Fast Fourier Transform to unscramble the noisy data to the correct distribution. To distinguish it from standard QECC, this method is referred to as distribution error correction (DEC).

Provided that the noise channel is Pauli (we can bias the noise towards Pauli through twirling [17]), the noisy distribution and the ideal distribution are related by a stochastic matrix \tilde{A} . We prove that the stochastic matrix \tilde{A} has a block circulant structure [18] and is thus described by a single column. This relation allows us to characterize \tilde{A} with a single circuit and reverse the error via the Fast Fourier Transform. Scaling can be straightforwardly achieved by truncating the vectors, which is also a method typically used to scale assignment matrix based error mitigation techniques [19, 20].

The results are corroborated by quantum hardware executions consisting of state preparation circuits for 20-qubit and 30-qubit GHZ states and 10-qubit and 20-qubit Dicke states with 1 excitation (the Dicke 10-1 and Dicke 20-1 states are denoted as $|D_1^{10}\rangle$ and $|D_1^{20}\rangle$, respectively). For the 30 qubit GHZ state preparation circuit, the output distribution is corrected to 97.7% fidelity from the initial raw fidelity of 23.2%. The quantum hardware executions also include 6-qubit and 10-qubit quantum phase estimation and 5-qubit Grover search and DEC achieves significant peaks on the correct basis states. The raw 5-qubit Grover search circuit consists of 582 CZ gates and DEC achieves a corrected fidelity of 74.9% from an initial raw fidelity of 10.2%. A summary of the fidelities and gate counts for the quantum hardware executions are provided in Tables I and II, respectively. Finally, we discuss open problems with DEC, possible solutions, and the relationship between DEC and assignment matrix based error mitigation methods.

II. BACKGROUND

Let X , Y , and Z denote the Pauli matrices. The Pauli group is defined as

$$\mathcal{P} = \{I, X, Y, Z\}^{\otimes n} \times \{\pm 1, \pm i\}. \quad (1)$$

* agonzales@anl.gov

An important class of unitary operations are Clifford operations, which maps the Pauli group into itself [1].

We also make extensive use of randomized compiling [21], which biases the noise affecting quantum gates towards a Pauli channel via twirling [17, 22]. Twirling is defined as

$$\mathcal{E}'(\rho) = \frac{1}{|T|} \sum_{i, (V \in T)} V E_i V^\dagger \rho V E_i^\dagger V^\dagger, \quad (2)$$

where T is the Twirling set and the E_i s are Kraus operators of the original noise channel.

Finally, given a payload circuit, a noise estimation circuit (NEC) is a constructed circuit with a similar structure [23]. The noise estimation circuit is typically used to estimate the errors affecting a quantum circuit.

III. RESULTS

We first prove important properties of the assignment matrix corresponding to a composite Pauli noise channel affecting a quantum circuit.

A. Quantum Circuit Error Assignment Matrix

For an arbitrary noisy unitary quantum circuit, we can write the evolution as an ideal unitary channel followed by a noise channel

$$\rho' = \mathcal{E} \circ \mathcal{U}(\rho) = \sum_i E_i U \rho U^\dagger E_i^\dagger \quad (3)$$

$$= \sum_i E_i \tilde{\rho} E_i^\dagger, \quad (4)$$

where $\mathcal{E}(\rho) = \sum_i E_i \rho E_i^\dagger$ is the noise channel, $\mathcal{U}(\rho) = U \rho U^\dagger$, U represents the circuit, and $\tilde{\rho} \equiv U \rho U^\dagger$. The rotations corresponding to the measurement basis are included in U . This description is general for completely positive noise channels. Note that $\tilde{\rho}$ is the ideal (noise free) state generated by the quantum circuit.

A simpler scenario arises when \mathcal{E} is biased into a Pauli noise channel. In this scenario, Eq. (4) becomes

$$\rho' = \sum_i \chi_i P_i \tilde{\rho} P_i, \quad (5)$$

where χ_i is real and P_i is from the set of $+1$ elements of the Pauli group. In the following analytical results, we constrain \mathcal{E} to Pauli.

Proposition 1. *Let the noise channel affecting the quantum circuit be Pauli. Then the noisy distribution \vec{z} and the ideal distribution \vec{x} in the standard basis are related by a stochastic matrix \tilde{A} , i.e., $\tilde{A}\vec{x} = \vec{z}$.*

The proof is provided in the Appendix. A similar result was proven for the more restricted case of measurement

errors in Ref. [24]. \tilde{A} is $2^n \times 2^n$ and stochastic. Notice that we do not need to characterize A , but only the submatrix \tilde{A} of A . Next, we describe symmetry properties of \tilde{A} that we use to characterize it with a single circuit and perform inversion in an efficient manner.

Proposition 2. *The elements of \tilde{A} are related by*

$$\langle j | \tilde{A} P_x | k \rangle = \langle j | P_x \tilde{A} | k \rangle \quad \forall |j\rangle, |k\rangle, P_x \quad (6)$$

where P_x is a Pauli X string.

The proof follows from the fact that Pauli channels commute. Since the proof requires notation used in the proof of Prop. 1 we also put this proof in the appendix.

Proposition 2, implies that \tilde{A} is completely characterized by *any one* of its columns, since all of the columns of \tilde{A} have the same elements, but reordered. Therefore, using Eq. (6) we only have to characterize one column of \tilde{A} to characterize all of \tilde{A} . Some important properties of \tilde{A} immediately follow from Prop. 2.

Corollary 1. *\tilde{A} is symmetric.*

Proof. This immediately follows from Prop. 2 by setting $|j\rangle = |k\rangle$. Then $\langle k | \tilde{A} | k' \rangle = \langle k' | \tilde{A} | k \rangle \forall |k'\rangle, |k\rangle$, where $|k'\rangle = P_x |k\rangle$. \square

Corollary 2. *\tilde{A} is doubly stochastic (i.e., each row and each column sums to 1).*

Proof. Consider the first column \vec{a} of \tilde{A} . From Prop. 2, each element of \vec{a} appears once in each column. Additionally, Prop. 2 implies that the row position of each element is different for each column. Thus, \tilde{A} is doubly stochastic. \square

Theorem 1. *\tilde{A} is composed of nested circulant 2×2 block matrices.*

Proof. \tilde{A} is $2^n \times 2^n$. Thus, it has an even number of rows and columns. We will recursively decompose \tilde{A} into 2×2 block matrices of equal sizes. Let i denote the layer of recursion. For $i = 0$,

$$\tilde{A} = \begin{bmatrix} B & C \\ D & E \end{bmatrix}, \quad (7)$$

where B, C , and D are $\frac{2^n}{2} \times \frac{2^n}{2}$ matrices. Let us write the (x, y) coordinates of each element of \tilde{A} in binary. Notice that the bit values at index $i = 0$ (i.e., the leftmost bit) for these coordinates are $(0,0)$, $(0,1)$, $(1,0)$, and $(1,1)$ for elements in B , C , D , and E , respectively. Let $P_x = X_0$ (Pauli X on qubit 0). Then directly applying Prop. 2 implies that $B = E$ and $C = D$. Thus,

$$\tilde{A} = \begin{bmatrix} B & C \\ C & B \end{bmatrix}, \quad (8)$$

which is block circulant. We can repeat this analysis for B and C , where we decompose B and C into 2×2

block matrices with each block being $\frac{2^n}{4} \times \frac{2^n}{4}$. Examining coordinates at bit index $i = 1$ and repeating the same analysis with $P_x = X_1$ and Prop. 2, yields that B and C are 2×2 block circulant. This pattern repeats until the final recursion of $i = n - 1$. \square

B. Inversion of \tilde{A}

In general \tilde{A} is not guaranteed to be invertible. However, due to its block circulant structure, we can easily construct its inverse or pseudo-inverse [18]. In our case, \tilde{A} is diagonalized by the tensor product of 2×2 Fourier Transform matrices, i.e., $H^{\otimes n}$. The system of equations given by $\tilde{A}\vec{x} = \vec{z}$, where \vec{x} is the ideal counts and \vec{z} is the noisy counts of the raw payload circuit, is solved by

$$\vec{x} = \text{IFWHT}(\text{FWHT}(\vec{z}) ./ \text{FWHT}(\vec{a})), \quad (9)$$

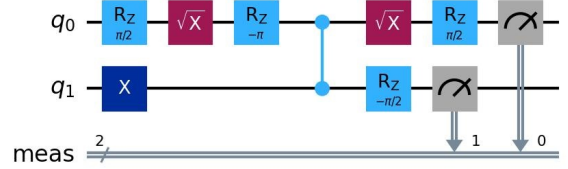
where \vec{a} is the first column of \tilde{A} , $./$ is element wise division, FWHT is the Fast Walsh-Hadamard transform, and IFWHT is the inverse FWHT. \vec{a} can be determined from any column of \tilde{A} through Eq. (6). For elements where a division by zero occurs, we can assign an element output of zero and this is the equivalent of performing the pseudo-inverse. Note that we should pad zero elements so that the basis states for \vec{a} and \vec{z} coincide. Additionally, we should pad with zeros for unoccupied basis states so that the dimensions of \vec{z} and \vec{a} are a power of 2. Eq. (9) is much faster than performing matrix inversion. The number of operations required is $O(m \log(m))$, where m is the dimension of the array. In contrast, matrix inversion scales $O(m^3)$.

Since $m = 2^n$ in general, we still run into exponential scaling. To handle this scenario, we can truncate \vec{z} and \vec{a} by keeping only the $m < 2^n$ largest values. This results in approximate correction, but as long as m is a polynomial function of n , DEC scales polynomially with the number of qubits. In the experiments, using Eq. (9) takes only a few seconds with array sizes of up to 2^{15} elements.

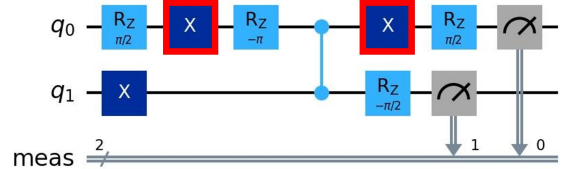
C. Characterization of \tilde{A} with Vanilla Noise Estimation Circuit

We now turn to characterization. As a warm up, we will first analyze a simple characterization scheme using a noise estimation circuit (NEC). This method is referred to as vanilla NEC. To perform characterization, we first transpile the circuit so that it complies with the gate set and connectivity of the quantum hardware device. Call this transpiled circuit the payload circuit. Without a loss of generality, let the gate set be given by CZ, SX, RZ, and X. Notice that the only gate capable of creating a superposition is SX

$$\text{SX} = \frac{1}{2} \begin{bmatrix} 1 & -i \\ -i & 1 \end{bmatrix}. \quad (10)$$



(a) Payload circuit.



(b) Noise estimation circuit.

FIG. 1. The NEC is constructed by replacing SX gates in the payload circuit with X gates (outlined in red). The NEC does not generate a superposition by construction and thus its ideal output when evolving from the ground state is a standard basis state $|k\rangle$ that we can efficiently determine classically.

We construct a noise estimation circuit (NEC) from the payload circuit by replacing SX gates with X gates while keeping everything else the same. An example of the NEC construction process is provided in Figs. 1a and 1b.

Next, we perform randomized compiling to bias the noise towards Pauli. Since the noise estimation circuit has a very similar circuit structure to the payload circuit, we make the assumption that its associated noise channel is very close to the one for the payload circuit. This assumption is corroborated, by previous experiments on noise estimation circuits [23] and this paper's quantum hardware results. Limitations and possible improvements of the described NEC for characterization of \tilde{A} are discussed in the next section and in Sec. IV.

Since the NEC does not create superposition when evolving from the ground state, it is easy to determine the ideal output $|k\rangle$ of the NEC classically, which corresponds to the column of \tilde{A} we are characterizing. Let the elements of column $|k\rangle$ of \tilde{A} be denoted by \vec{b} . \vec{b} is generated by sampling the NEC. Then, the first column vector \vec{a} can be determined by application of Eq. (6).

D. Improved Characterization

In vanilla NEC we replace SX with X. SX maps Y to Z and thus can cause the Pauli channel of the NEC circuit to deviate from the payload circuit. However, notice that if the SX gates appear at the beginning of the circuit, this scenario does not occur since there are no gates before

them. Thus, before constructing the NEC, we should commute the SX gates as close to the beginning of the circuit as possible in the payload circuit. Ideally, we want to achieve a circuit structure of \mathbf{SN} , where \mathbf{S} consists only of SX gates and \mathbf{N} does not contain SX.

For a general basis, we want the gate(s) being replaced for the construction of the NEC circuit to appear in the beginning. For Clifford payload circuits this structure is always possible in the $\{\text{H}, \text{CX}, \text{CZ}, \text{P}\}$ basis, since a Clifford operation admits a $\mathbf{F}_1 \mathbf{H} \mathbf{F}_2$ decomposition, where \mathbf{F}_i cannot create superposition [25, 26]. Thus, we can use this structure by replacing H, which is the only gate that creates superposition, in the construction of the NEC. Since the circuit is Clifford and we are evolving from the ground state, \mathbf{F}_1 only introduces a global phase and can be replaced with identity. Since \mathbf{H} consists only of H gates, we satisfy the structure. We leave implementation of the improved characterization for future work.

E. Quantum Hardware and Simulation Results

The following are the results for the experiments conducted for this paper. The quantum hardware results were executed on `ibm_marrakesh` with 200,000 shots each for the NEC and the payload circuit. The sizes of the vectors are truncated to a maximum size of 2^{15} . Unless stated otherwise, the simulations used 0.001 and 0.01 single qubit and two qubit depolarization rates, respectively. The simulations also assume full connectivity. The corrected distributions are in general quasi-distributions since they can contain negative values. To correct to a near distribution, the method described in Ref. [27] is used. Results for 20-qubit and 30-qubit GHZ state preparation, $|D_1^{10}\rangle$ and $|D_1^{20}\rangle$ state preparation, 6-qubit and 10-qubit quantum phase estimation (QPE), and 5 qubit Grover search are presented. An overview of the fidelities and gate counts of the quantum hardware results are provided in Tables I and II, respectively.

1. Clifford Circuits

The following are GHZ state preparation circuits which are Clifford. Randomized compiling biases the error channels associated with each layer of the circuit towards Pauli. Since the entire circuit is Clifford and Clifford gates map Paulis to Paulis, the composite noise channel affecting the entire circuit is close to Pauli. The highlight result is the 30-qubit GHZ quantum hardware execution that achieves 97.7% fidelity as shown in Fig. 2. The result of the 20-qubit GHZ experiment is shown in Fig. 3. The corrected distribution fidelity is 93.7%. Interestingly, the corrected 30-qubit GHZ experiment achieves a higher fidelity despite the larger number of gates and qubits. The lack of unit fidelity can be attributed to issues such as shot noise, deviation from the Pauli bias,

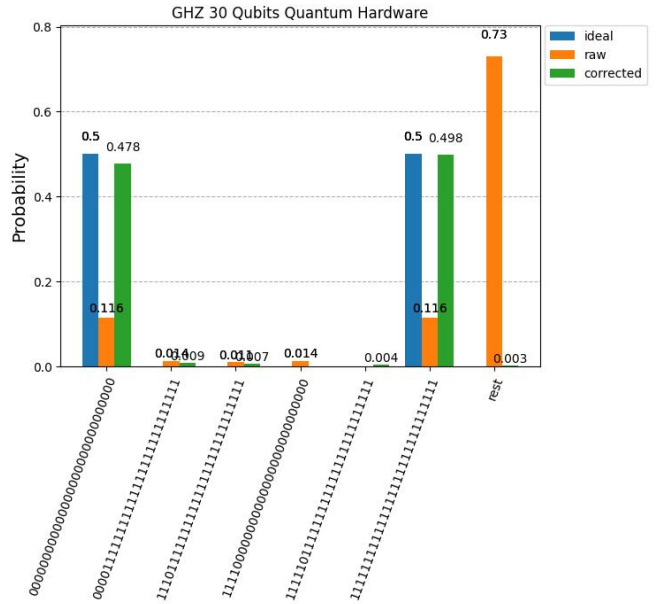


FIG. 2. GHZ 30 Qubits on quantum hardware.

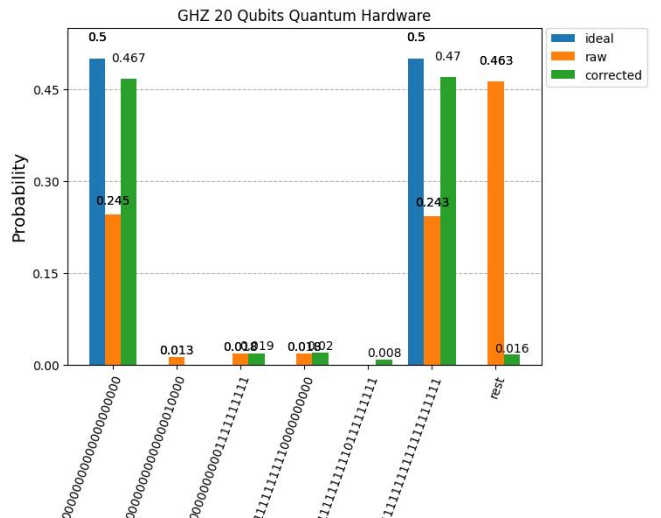


FIG. 3. GHZ 20 qubits on quantum hardware.

and differences between the noise channels of the NEC and the raw circuit.

2. Non-Clifford Circuits

We now turn to non-Clifford circuits. In contrast to Clifford circuits, the presence of non-Clifford gates can destroy the biasing towards Pauli since they can in general map Paulis to non-Paulis. Still, as the following results show, DEC is tolerant to some level of deviation from the Pauli bias. We first discuss the preparation of Dicke states. The sparse state preparation method in Ref. [28] was used to generate the Dicke state prepara-

	Fidelities						
	GHZ-20	GHZ-30	Dicke n=10, k=1	Dicke n=20, k=1	QPE-6	QPE-10	Grover-5
Corrected	0.937	0.977	0.935	0.803	0.897	0.326	0.749
Raw	0.488	0.232	0.576	0.283	0.579	0.029	0.102

TABLE I. Fidelities for circuits executed on quantum hardware. Raw corresponds to the output of the original circuit without correction. Corrected corresponds to the corrected distribution via DEC. The dash followed by a number specifies the number of qubits used.

	Payload Circuit Gate Counts						
Gate	GHZ-20	GHZ-30	Dicke n=10, k=1	Dicke n=20, k=1	QPE-6	QPE-10	Grover-5
CZ	19	29	18	38	77	267	582
RZ	59	89	45	95	91	259	742
SX	39	59	50	100	158	556	1281
X	0	0	1	6	5	9	48

TABLE II. Gate counts for the raw payload circuits executed on quantum hardware. The dash followed by a number specifies the number of qubits used.

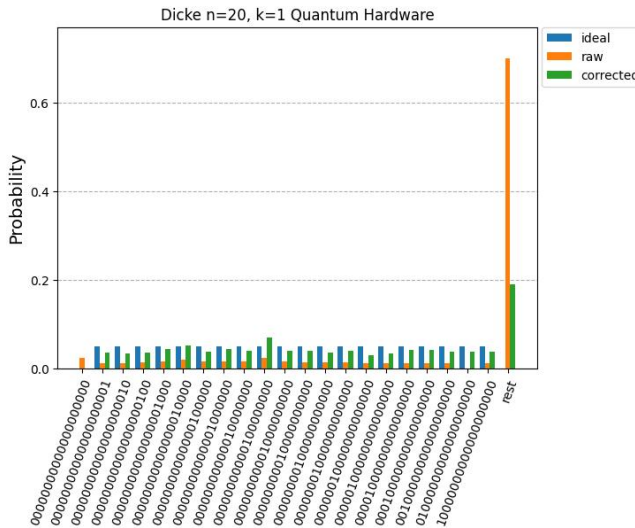


FIG. 4. Dicke $|D_1^{20}\rangle$ state preparation on quantum hardware.

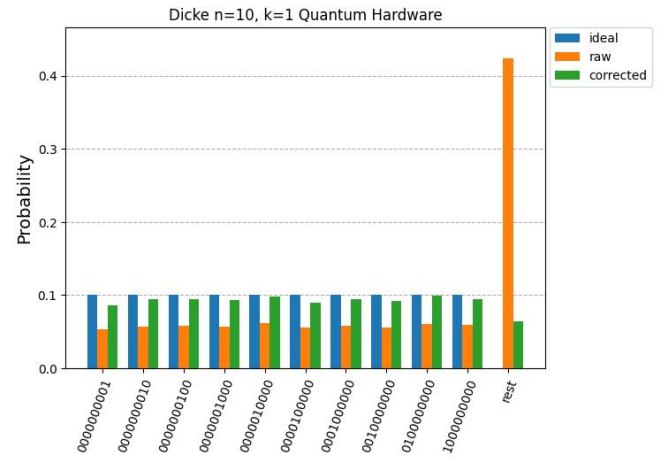


FIG. 5. Dicke $|D_1^{10}\rangle$ state preparation on quantum hardware.

IV. OPEN PROBLEMS AND FUTURE DIRECTIONS

There are two key factors for executing DEC effectively: (1) Pauli bias for the *composite* noise channel (see Eq. (5)) and (2) accurate characterization of \vec{a} . Still, the quantum hardware results show that DEC is resilient to some level of deviation from these criteria. For Clifford circuits, (1) is relatively easy to achieve. For non-Clifford circuits, we can bias the noise channels after each gate to Pauli using twirling. However, the composite channel will in general be non-Pauli since some of the Pauli channels will pass through non-Clifford gates.

A possible solution to this issue is magic state injection [29]. In this scenario, aside from the the magic state preparation circuits, the dynamic circuit is completely Clifford. However, the behavior of the composite noise channel is unclear since we are now dealing with an ensemble of circuits.

For criteria (2), the vanilla NEC method, while sim-

tion circuits. As shown in Fig. 4, the rest bar, which can be interpreted as an approximation of the infidelity, is significantly higher than the corrected rest bar. Figure 5 shows the results for $|D_1^{10}\rangle$.

Next, the results for the quantum phase estimation experiments are shown in Figs. 6a, 6b, 7a, and 7b. The simulated results are Figs. 6b and 7b. The phase angles were chosen to be $\theta = \frac{31}{32}$ and $\theta = \frac{511}{512}$ to correspond with a peak value of all 1s for the 6 and 10 qubit experiments, respectively. Finally, the Grover search experiments on 5 qubits were conducted with a target state of all 1s. The optimal number of iterations were used. The results are shown Figs. 8a and 8b with the latter from simulation.

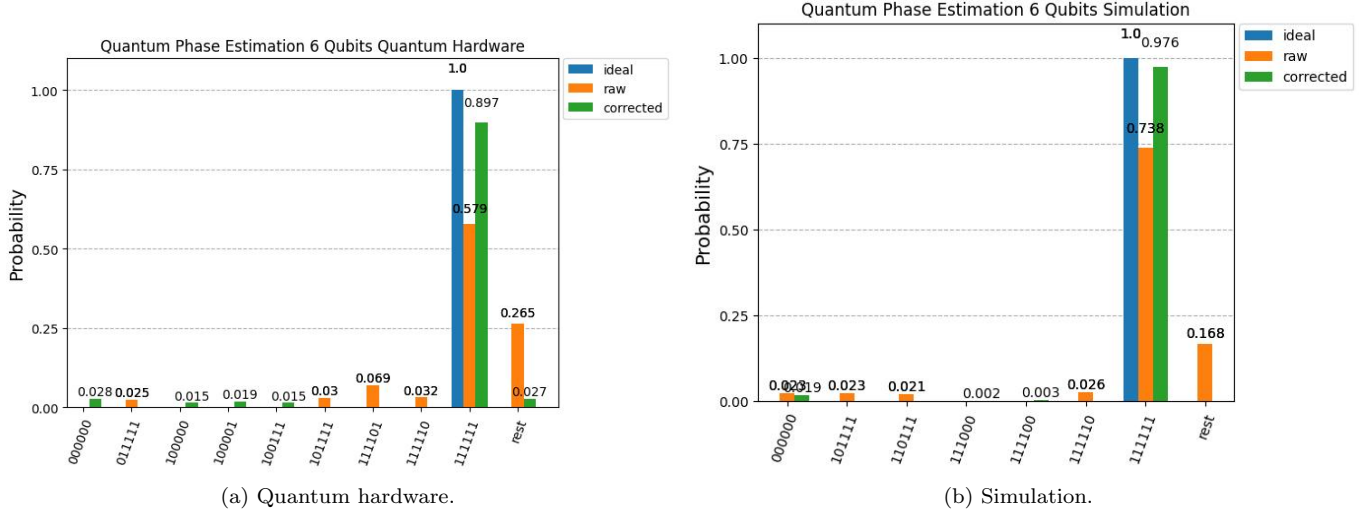


FIG. 6. The phase angle used is $\theta = \frac{31}{32}$ which corresponds to an ideal output of all 1s. Note that the control qubit is included in the correction. There is a clear peak at the correct value for both quantum hardware and simulation.

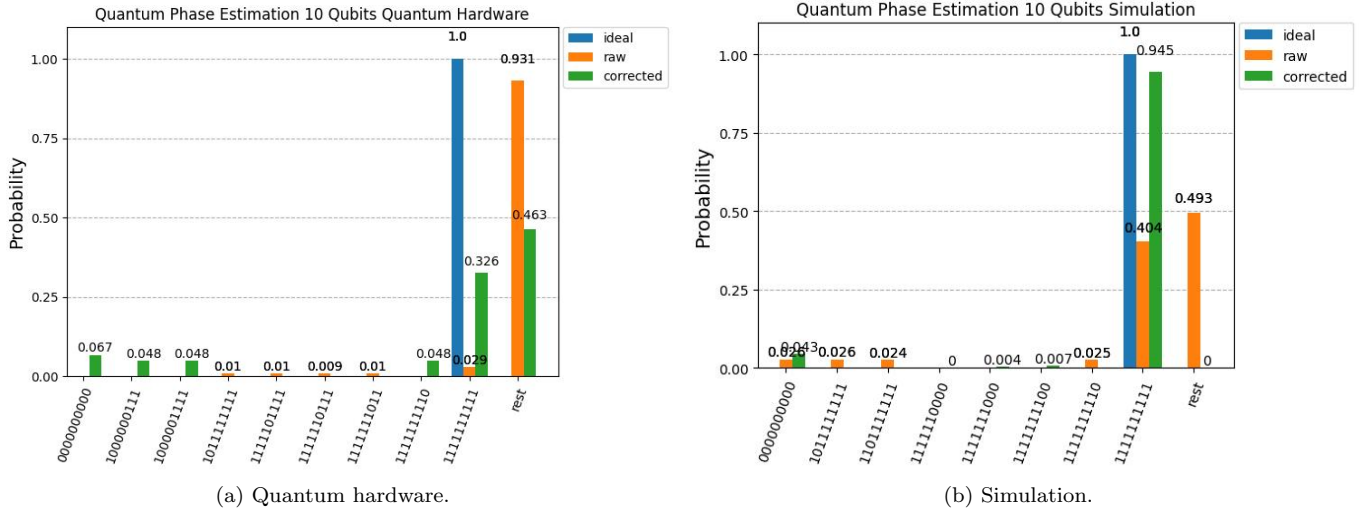


FIG. 7. The phase angle used is $\theta = \frac{511}{512}$ which corresponds to an ideal output of all 1s. Note that the control qubit is included in the correction. There is a clear peak at the correct value for both quantum hardware and simulation.

ple to implement, does not always accurately generate \vec{a} . In vanilla NEC, we replace SX gates with X gates in the NEC. The differences in the noise channels can occur because in the payload circuit the noise channels transform through SX gates and in the NECs noise channels transform through X gates. The improved NEC characterization described in Sec. III D will probably help a lot in solving this problem. The timing of the sampling of the NEC and payload circuit is also important. These should be sampled close together to avoid noise drift.

An important line of investigation that would help in satisfying these criteria is improving twirling methods. For instance, it is likely that we should use the same twirls for both the payload circuit and NEC. Addition-

ally, performing twirling of the whole circuit solves a lot of the previously discussed issues since the composite channel will be depolarizing. However, how to do this efficiently and for general circuits is an open problem.

Next, the dimension of \vec{a} will generally increase with the number of qubits. The naive way to deal with this is with truncation. However, this might not be the best approach. A different approach is to segment \vec{a} into a tensor product, but how to do this in a clever fashion needs more work. Lastly, applying DEC in combination with QECC or other techniques such as noise aware qubit mapping [30] are interesting open questions.

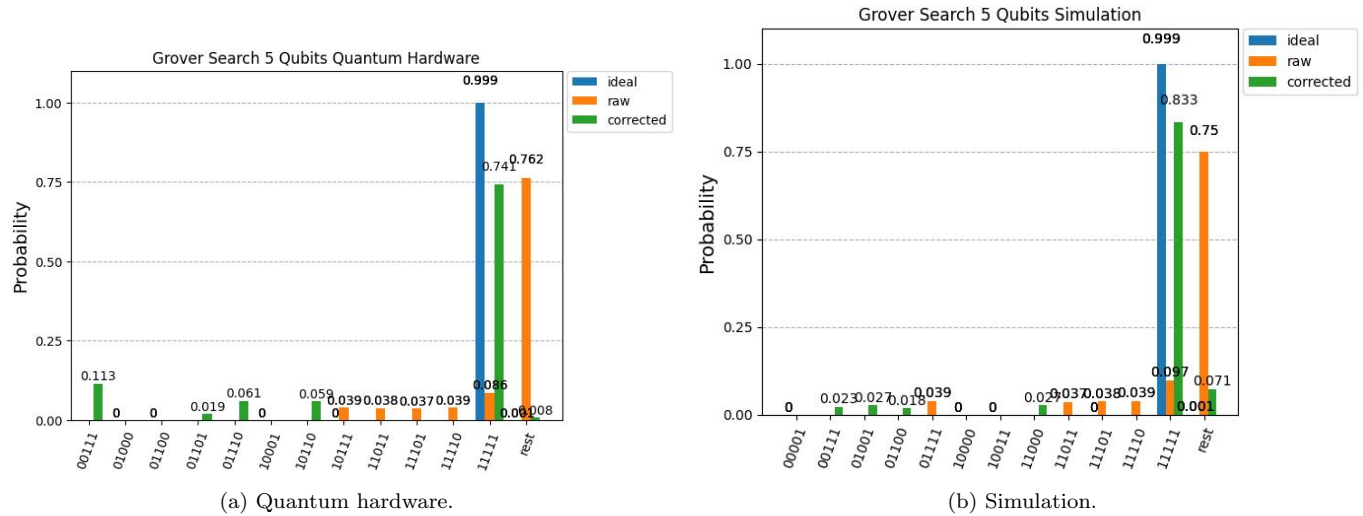


FIG. 8. Grover Search. The ideal state is 11111.

V. CONCLUSIONS

This work introduces DEC, which is a novel quantum error correction method that focuses on correcting the output distribution and does not require encoding of logical states into a larger number of physical qubits. Thus, DEC does not incur the overhead of QECC. We prove that Pauli noise channels generate a circulant assignment matrix and leverage this to correct the noisy output distribution via the Fast Fourier Transform. Additionally, an efficient way to characterize the noise assignment matrix, which requires sampling only a single circuit, is provided. The experimental results on quantum hardware show significant fidelity improvements for GHZ, quantum phase estimation, Grover Search, and Dicke state preparation. For 30-qubit GHZ, a corrected fidelity of 97.7% is achieved. The initial raw fidelity was 23.2%.

The error mitigation techniques of general error mitigation [10, 20] and measurement error mitigation [9, 19] use inversion of an assignment matrix. DEC significantly differs from these methods. In measurement error mitigation, the assignment matrix is only characterized for the measurement errors. In general error mitigation, the method explicitly avoids noise biasing. In both of these methods, a circulant structure is not known and the columns of the assignment matrix are independently characterized. Thus, the Fast Fourier Transform is not used for inversion. DEC encompasses measurement error mitigation when measurement errors are biased to Pauli.

VI. DATA AVAILABILITY

The data presented in this paper is available online at https://github.com/alvinquantum/quantum_error_correction_without_encoding.

VII. ACKNOWLEDGEMENTS

I thank Daniel Dilley and Zain H. Saleem from Argonne National Laboratory for useful discussions. This material is based upon work supported by Laboratory Directed Research and Development (LDRD) funding from Argonne National Laboratory, provided by the Director, Office of Science, of the U.S. Department of Energy under Contract No. DE-AC02-06CH11357. This research used resources of the Oak Ridge Leadership Computing Facility, which is a DOE Office of Science User Facility supported under Contract DE-AC05-00OR22725.

Appendix A: Proof of Prop. 1

Proof. Let $\tilde{\rho} = \sum_{lr} \alpha_{lr} |l\rangle\langle r|$ in the standard basis and measurements be in the standard basis. Measurement in the standard basis yields the output distribution

$$P(k|\rho') = \text{tr}(|k\rangle\langle k| \rho') \quad (\text{A1})$$

$$= \text{tr}\left(|k\rangle\langle k| \sum_i \chi_i P_i \sum_{lr} \alpha_{lr} |l\rangle\langle r| P_i\right). \quad (\text{A2})$$

Since the expansion and the measurement are in the standard basis and Pauli operators map standard basis elements to standard basis elements, only the diagonal components of $\tilde{\rho}$ contribute to the probabilities. Thus,

$$P(k|\rho') = \text{tr}\left(|k\rangle\langle k| \sum_i \chi_i P_i \sum_l \alpha_{ll} |l\rangle\langle l| P_i\right). \quad (\text{A3})$$

This can also be written in terms of vectors \square

$$P(k|\rho') = \langle kk| \text{vec}(\rho') = \langle kk| \sum_i \chi_i P_i^T \otimes P_i \text{vec}(\tilde{\rho}) \quad (\text{A4})$$

$$= \langle kk| A \sum_l \alpha_{ll} |ll\rangle \quad (\text{A5})$$

where $A \equiv \sum_i \chi_i P_i^T \otimes P_i \equiv \sum_{ijkl} a_{ijkl} |ij\rangle\langle kl|$. Since A maps diagonal components to diagonal components and off diagonal terms to off diagonal, the only part of A that contributes to a measurement outcome in the standard basis is $\tilde{A} = \sum_{ir} a_{iirr} |ii\rangle\langle rr|$ and we have

$$P(k|\tilde{\rho}) = \langle kk| \tilde{A} \sum_l \alpha_{ll} |ll\rangle. \quad (\text{A6})$$

Then we can construct a vector of the outcomes

$$P(k|\tilde{\rho}) |kk\rangle = \tilde{A} \sum_l \alpha_{ll} |ll\rangle. \quad (\text{A7})$$

We can write this in a more compact form by letting $ii \rightarrow i$

$$\tilde{P}(k|\tilde{\rho}) |kk\rangle = \sum_{ir} a_{iirr} |ii\rangle\langle rr| \sum_l \alpha_{ll} |ll\rangle : \rightarrow \quad (\text{A8})$$

$$P(k|\tilde{\rho}) |k\rangle = \tilde{A} \sum_l \alpha_l |l\rangle \quad (\text{A9})$$

where

$$\tilde{A} = \sum_{ir} a_{ir} |i\rangle\langle r|. \quad (\text{A10})$$

Appendix B: Proof of Prop. 2

Proof. Since Pauli channels commute, we can write

$$\sum_i \chi_i P_i P_x \rho P_x P_i = \sum_i \chi_i P_x P_i \rho P_i P_x, \quad \forall P_x \quad (\text{B1})$$

\rightarrow

$$(P_x \otimes P_x) A = A (P_x \otimes P_x), \quad \forall P_x, \quad (\text{B2})$$

where P_x is a Pauli X string. Thus,

$$\tilde{A} P_x = P_x \tilde{A}, \quad \forall P_x \quad (\text{B3})$$

\rightarrow

$$\langle j| \tilde{A} P_x |k\rangle = \langle j| P_x \tilde{A} |k\rangle \quad \forall |j\rangle, |k\rangle, P_x. \quad (\text{B4})$$

\square

The submitted manuscript has been created by UChicago Argonne, LLC, Operator of Argonne National Laboratory (“Argonne”). Argonne, a U.S. Department of Energy Office of Science laboratory, is operated under Contract No. DE-AC02-06CH11357. The U.S. Government retains for itself, and others acting on its behalf, a paid-up nonexclusive, irrevocable worldwide license in said article to reproduce, prepare derivative works, distribute copies to the public, and perform publicly and display publicly, by or on behalf of the Government. The Department of Energy will provide public access to these results of federally sponsored research in accordance with the DOE Public Access Plan. <http://energy.gov/downloads/doe-public-access-plan>.

[1] Michael A Nielsen and Isaac L Chuang. *Quantum Computation and Quantum Information*. Cambridge University Press, 2011.

[2] P. W. Shor. Fault-tolerant quantum computation. In *Proceedings of the 37th Annual Symposium on Foundations of Computer Science*, FOCS '96, page 56, USA, 1996. IEEE Computer Society.

[3] Daniel Gottesman. Stabilizer codes and quantum error correction, 1997.

[4] Dorit Aharonov and Michael Ben-Or. Fault-tolerant quantum computation with constant error rate. *SIAM Journal on Computing*, 38(4):1207–1282, 2008.

[5] Acharya et. al. Quantum error correction below the surface code threshold. *Nature*, Dec 2024.

[6] Austin G. Fowler, Matteo Mariantoni, John M. Martinis, and Andrew N. Cleland. Surface codes: Towards practical large-scale quantum computation. *Phys. Rev. A*, 86:032324, Sep 2012.

[7] Christopher Chamberland, Tomas Jochym-O’Connor, and Raymond Laflamme. Overhead analysis of universal concatenated quantum codes. *Physical Review A*, 95(2), February 2017.

[8] Earl T. Campbell, Barbara M. Terhal, and Christophe Vuillot. Roads towards fault-tolerant universal quantum computation. *Nature*, 549(7671):172–179, September 2017.

[9] Filip B. Maciejewski, Zoltán Zimborás, and Michał Oszmaniec. Mitigation of readout noise in near-term quantum devices by classical post-processing based on detector tomography. *Quantum*, 4:257, April 2020.

[10] Manpreet Singh Jattana, Fengping Jin, Hans De Raedt, and Kristel Michelsen. General error mitigation for quantum circuits. *Quantum Information Processing*, 19(11), November 2020.

[11] Jarrod R. McClean, Mollie E. Kimchi-Schwartz, Jonathan Carter, and Wibe A. de Jong. Hybrid quantum-classical hierarchy for mitigation of decoherence and determination of excited states. *Phys. Rev. A*, 95:042308, Apr 2017.

[12] Ying Li and Simon C. Benjamin. Efficient variational quantum simulator incorporating active error minimization. *Phys. Rev. X*, 7:021050, Jun 2017.

[13] Kristan Temme, Sergey Bravyi, and Jay M. Gambetta. Error mitigation for short-depth quantum circuits. *Physical Review Letters*, 119(18), November 2017.

[14] Dripto M. Debroy and Kenneth R. Brown. Extended flag gadgets for low-overhead circuit verification. *Physical Review A*, 102(5), November 2020.

- [15] Alvin Gonzales, Ruslan Shaydulin, Zain H. Saleem, and Martin Suchara. Quantum error mitigation by pauli check sandwiching. *Scientific Reports*, 13(1), February 2023.
- [16] William J. Huggins, Sam McArdle, Thomas E. O'Brien, Joonho Lee, Nicholas C. Rubin, Sergio Boixo, K. Birgitta Whaley, Ryan Babbush, and Jarrod R. McClean. Virtual distillation for quantum error mitigation. *Phys. Rev. X*, 11:041036, Nov 2021.
- [17] Zhenyu Cai and Simon C. Benjamin. Constructing smaller pauli twirling sets for arbitrary error channels. *Scientific Reports*, 9(1), August 2019.
- [18] Mansoor Rezghi and Lars Eldén. Diagonalization of tensors with circulant structure. *Linear Algebra and its Applications*, 435(3):422–447, 2011. Special Issue: Dedication to Pete Stewart on the occasion of his 70th birthday.
- [19] Paul D. Nation, Hwajung Kang, Neereja Sundaresan, and Jay M. Gambetta. Scalable mitigation of measurement errors on quantum computers. *PRX Quantum*, 2:040326, Nov 2021.
- [20] Philip Döbler, Jannik Pfleiger, Fengping Jin, Hans De Raedt, Kristel Michelsen, Thomas Lippert, and Manpreet Singh Jattana. Scalable general error mitigation for quantum circuits, 2024.
- [21] Joel J. Wallman and Joseph Emerson. Noise tailoring for scalable quantum computation via randomized compiling. *Physical Review A*, 94(5), November 2016.
- [22] Charles H. Bennett, David P. DiVincenzo, John A. Smolin, and William K. Wootters. Mixed-state entanglement and quantum error correction. *Phys. Rev. A*, 54:3824–3851, Nov 1996.
- [23] Miroslav Urbanek, Benjamin Nachman, Vincent R. Paszczuzzi, Andre He, Christian W. Bauer, and Wibe A. de Jong. Mitigating depolarizing noise on quantum computers with noise-estimation circuits. *Physical Review Letters*, 127(27), December 2021.
- [24] Michael R Geller. Rigorous measurement error correction. *Quantum Science and Technology*, 5(3):03LT01, June 2020.
- [25] Dmitri Maslov and Martin Roetteler. Shorter stabilizer circuits via bruhat decomposition and quantum circuit transformations. *IEEE Transactions on Information Theory*, 64(7):4729–4738, July 2018.
- [26] Sergey Bravyi and Dmitri Maslov. Hadamard-free circuits expose the structure of the clifford group. *IEEE Transactions on Information Theory*, 67(7):4546–4563, July 2021.
- [27] John A. Smolin, Jay M. Gambetta, and Graeme Smith. Efficient method for computing the maximum-likelihood quantum state from measurements with additive gaussian noise. *Phys. Rev. Lett.*, 108:070502, Feb 2012.
- [28] Alvin Gonzales, Rebekah Herrman, Colin Campbell, Igor Gaidai, Ji Liu, Teague Tomesh, and Zain H. Saleem. Efficient sparse state preparation via quantum walks, 2024.
- [29] Xinlan Zhou, Debbie W. Leung, and Isaac L. Chuang. Methodology for quantum logic gate construction. *Physical Review A*, 62(5), October 2000.
- [30] Quinn Langfitt, Alvin Gonzales, Joshua Gao, Ji Liu, Zain H. Saleem, Nikos Hardavellas, and Kaitlin N. Smith. Dynamic resource allocation with quantum error detection, 2024.